Contribution from the Department of Chemistry, The University of Houston, Houston, Texas 77004, and Laboratoire de Synthèse et d'Electrosynthèse, Organométallique associé au CNRS (UA 33), Faculté des Sciences "Gabriel", 21100 Dijon, France

Reactions of Metalloporphyrins Possessing Metal–Metal Bonds. Synthesis and Electrochemical Studies of $(P)Sn^{II}Fe(CO)_4$ and $(P)Ge^{II}Fe(CO)_4$, Where P = Octaethylporphyrin or Tetraarylporphyrin

K. M. Kadish,*[1a] C. Swistak,[1a] B. Boisselier-Cocolios,[1a] J. M. Barbe,[1b] and R. Guilard*[1b]

Received March 7, 1986

The synthesis and characterization of $(P)SnFe(CO)_4$ and $(P)GeFe(CO)_4$ is reported for P = octaethylporphyrin or tetraarylporphyrin. Metal–metal complexes of $(P)MFe(CO)_4$, where M = Sn(II) or Ge(II), were synthesized by the reaction of $Na_2Fe(CO)_4$ with the corresponding $(P)M^{IV}Cl_2$ complex in THF. The final products were purified and characterized by ^1H NMR, IR, UV–visible, and mass spectroscopy and electrochemistry. All of the bimetallic complexes were extremely stable after electroreduction, and two reversible one-electron-transfer steps could be observed without cleavage of the metal–metal bond. These reductions occurred at the π ring system of the metalloporphyrin. In contrast, each $(P)MFe(CO)_4$ complex underwent an initial irreversible oxidation at the central metal, which led to $[(P)M^{IV}]^{2+}$ and $Fe_3(CO)_{12}$ as the main products of electrooxidation. A self-consistent mechanism for the coupled chemical and electrochemical steps in the electrooxidation is presented.

Introduction

The synthesis of linear polymers having covalently bonded metal atoms has attracted a great deal of interest due to their potential superconductor properties.[2,3] These linear polymers should exhibit electron-transfer properties that depend on the metal-chain framework. In this regard, several new classes of metalloporphyrins having metal–metal bonds or implying a metal–metal interaction have recently been reported in the literature.[4–15] Our interest in these types of complexes stems from the expectation that both the porphyrin ligand and the metal ion properties would combine to direct the type of electron transport and, as such, provide models for metal–metal-bonded reactions in linear-metal-chain derivatives.

In this paper, we present the redox properties of germanium and tin metalloporphyrins that are bound to an $Fe(CO)_4$ ion.[12] These donor–acceptor complexes are represented as (P)MM'L, where P is the octaethylporphyrin dianion (OEP^{2-}), *meso*-tetra-*p*-tolylporphyrin dianion ($TpTP^{2-}$), or *meso*-tetra-*m*-tolylporphyrin dianion ($TmTP^{2-}$), M is Sn or Ge, and M'L is $Fe(CO)_4$. Preliminary characterizations of these compounds have been published,[12,13] and an X-ray structure of $(OEP)SnFe(CO)_4$ has been obtained.[12] This compound has also been examined by IR and Mössbauer spectra, and on the basis of these data, Sn(II) and Fe(0) oxidation states have been assigned.[12] By analogy, the $(P)GeFe(CO)_4$ complexes are also postulated to have the main-group metal in a low oxidation state and, as such, the metalloporphyrin would contain a Ge(II)–Fe(0) metal–metal bond.

For the specific case of metalloporphyrins, Sn(II) and Ge(II) oxidation states are extremely uncommon. In fact, no Ge(II) porphyrins have ever been reported. Several spectral characterizations of $(OEP)Sn^{II}$[16] and $(TPP)Sn^{II}$[17] have appeared in the literature, but it is only recently that a genuine sample of an air-stable $(TPP)Sn^{II}$ complex has been isolated.[18] Thus, the carbenoid metal–metal-bonded metalloporphyrin complexes are unique in that the main-group metal is air-stable in the low oxidation state.

Experimental Section

The synthesis and handling of the metalloporphyrins and the tetracarbonyl dianions were carried out under an atmosphere of argon or nitrogen. All common solvents were thoroughly dried in a manner appropriate to each and were distilled under argon prior to use. All operations were carried out in Schlenk tubes with dried oxygen-free solvents under purified argon.

Synthesis. $(P)MFe(CO)_4$ complexes, where M = Sn(II) or Ge(II), were synthesized by the reaction of $Na_2Fe(CO)_4$ with the corresponding $(P)M^{IV}Cl_2$ complex in THF. The following preparation of $(OEP)SnFe(CO)_4$ illustrates the details of the reaction procedure.

[(2,3,7,8,12,13,17,18-Octaethylporphyrinato)tin(II)]tetracarbonyliron. A 0.67-mmol amount of $(OEP)Sn^{IV}Cl_2$ was added to a solution of 0.67 mmol of $Na_2Fe(CO)_4$ in THF (180 mL), and the mixture, with stirring, was allowed to stand at room temperature over a period of 24 h. The solution was then evaporated to dryness under vacuum, and the residual solid was purified by chromatography on an aluminum oxide column (eluant toluene). Evaporation of the eluant resulted in an orange-red solid, which was recrystallized from 25 mL of toluene to give 0.25 g (46% yield) of $(OEP)SnFe(CO)_4$. The conditions, yields, and spectroscopic data of the six synthesized complexes are summarized in Tables I–III.

Physical Measurements. Elemental analyses were performed by the "Service de Microanalyses du CNRS". Mass spectra were recorded in the electron-impact mode with a Finnigan 3300 spectrometer: ionizing energy 70 eV; ionizing current 0.4 mA; source temperature 250–400 °C. ^1H NMR spectra were recorded on a JEOL FX 100 spectrometer. Spectra were measured for complex solutions in 0.5 mL of C_5D_5N or C_6D_6 with use of tetramethylsilane as internal reference. Twenty to two hundred scans over 16K points were accumulated for each spectrum at 21 ± 1 °C. Infrared spectra were achieved on a Perkin-Elmer 580 B instrument. Samples were 10% dispersions in Nujol mulls. Electronic absorption spectra were performed on a Perkin-Elmer 559 spectrophotometer in toluene solutions.

ESR spectra were recorded on an IBM Model ER 100D spectrometer equipped with an ER-040-X microwave bridge and an ER 080 power supply. Cyclic voltammetric measurements were carried out with either an EG&G Model 173 potentiostat and an EG&G Model 175 universal programmer or a BAS 100 electrochemical analyzer. Current–voltage curves were recorded on a Houston Instruments Model 2000 X-Y recorder, a Houston Instruments HIPLOT DMP-40 plotter, or an Epson Model FX80 printer. A three-electrode system was used with a Pt-button or a gold working electrode and a Pt-wire counter electrode. A saturated

(1) (a) The University of Houston. (b) University of Dijon.
(2) Pitt, C. G.; Monteith, L. K.; Ballard, L. F.; Collman, J. P.; Morrow, J. C.; Roper, W. R.; Ulku, D. *J. Am. Chem. Soc.* **1966**, *88*, 4286.
(3) Interrante, L. V., Ed. *Extended Interactions between Metal Ions in Transition Metal Complexes*; ACS Symposium Series 5, American Chemical Society: Washington, DC, 1974; p 5, and references cited therein.
(4) Onaka, S.; Kondo, Y.; Toriumi, K.; Itoh, T. *Chem. Lett.* **1980**, 1605.
(5) Ibers, J. A.; Pace, L. J.; Martinsen, J.; Hoffman, B. M. *Struct. Bonding (Berlin)* **1983**, *50*, 1.
(6) Hoffman, B. M.; Ibers, J. A. *Acc. Chem. Res.* **1983**, *16*, 15.
(7) Cocolios, P.; Moise, C.; Guilard, R. *J. Organomet. Chem.* **1982**, *228*, C43.
(8) Cocolios, P.; Chang, D.; Vittori, O.; Guilard, R.; Moise, C.; Kadish, K. M. *J. Am. Chem. Soc.* **1984**, *106*, 5724.
(9) Wayland, B. B.; Newman, A. R. *Inorg. Chem.* **1981**, *20*, 3093.
(10) Collman, J. P.; Barnes, C. E.; Collins, T. J.; Brothers, P. J.; Gallucci, J.; Ibers, J. A. *J. Am. Chem. Soc.* **1981**, *103*, 7030.
(11) Collman, J. P.; Barnes, C. E.; Swepston, P. N.; Ibers, J. A. *J. Am. Chem. Soc.* **1984**, *106*, 3500.
(12) Barbe, J. H.; Guilard, R.; Lecomte, C.; Gerardin, R. *Polyhedron* **1984**, *3*, 889.
(13) Kadish, K. M.; Boisselier-Cocolios, B.; Swistak, C.; Barbe, J. M.; Guilard, R. *Inorg. Chem.* **1986**, *26*, 121.
(14) Brothers, P. J.; Collman, J. P. *Acc. Chem. Res.* **1986**, *19*, 209.
(15) Jones, N. L.; Carroll, P. J.; Wayland, B. B. *Organometallics* **1986**, *5*, 33.
(16) Whitten, D. G.; Yau, J. C.; Carroll, F. A. *J. Am. Chem. Soc.* **1971**, *93*, 2291.
(17) Edwards, L.; Dolphin, D.; Gouterman, M.; Adler, A. D. *J. Mol. Spectrosc.* **1971**, *38*, 16.
(18) Landrum, J. T.; Amini, M.; Zuckerman, J. J. *Inorg. Chim. Acta* **1984**, *90*, L73.

0020-1669/86/1325-4336$01.50/0

Table I. Characteristics of Reactions, Elemental Analyses, and Mass Spectral Data

complex[a]	recrystallizn solvent[b]	yield, %	Anal., %[c] C	H	N	Sn (or Ge)	Fe	mass spectra *m/e*	rel intens	fragmentation pattern
(OEP)SnFe(CO)$_4$	A	46	58.5	5.3	6.8	14.3	6.7	652	100.00	[(OEP)Sn]$^+$
			(58.64)	(5.41)	(6.84)	(14.49)	(6.82)	708	25.00	[(OEP)Sn–Fe]$^+$
(TpTP)SnFe(CO)$_4$	1/1 A/B	48	66.3	3.9	5.7	11.5	5.8	724	100.00	[(TpTP)Fe]$^+$
			(65.37)	(3.80)	(5.86)	(12.42)	(5.85)	788	89.47	[(TpTP)Sn]$^+$
								845	26.31	[(TpTP)Sn–Fe + H]$^+$
(TmTP)SnFe(CO)$_4$	1/2 A/B	45	64.9	3.8	5.7	11.3	5.6	724	61.79	[(TmTP)Fe]$^+$
			(65.37)	(3.80)	(5.86)	(12.42)	(5.85)	788	100.00	[(TmTP)Sn]$^+$
								844	4.48	[(TmTP)Sn–Fe]$^+$
								956	0.10	[(TmTP)Sn–Fe(CO)$_4$]$^+$
(OEP)GeFe(CO)$_4$	A	14	62.1	5.9	6.9	9.5	6.9	662	100.00	[(OEP)Ge–Fe]$^+$
			(62.13)	(5.74)	(7.25)	(9.39)	(7.22)	746	0.76	[(OEP)Ge–Fe(CO)$_3$]$^+$
								774	2.29	[(OEP)Ge–Fe(CO)$_4$]$^+$
(TpTP)GeFe(CO)$_4$	1/1 A/B	29	68.7	4.0	5.9	7.2	5.7	724	100.00	[(TpTP)Fe]$^+$
			(68.69)	(3.99)	(6.16)	(7.98)	(6.14)	742	13.12	[(TpTP)Ge]$^+$
								799	31.00	[(TpTP)Ge–Fe + H]$^+$
								882	0.84	[(TpTP)Ge–Fe(CO)$_3$]$^+$
								911	0.63	[(TpTP)Ge–Fe(CO)$_4$ + H]$^+$
(TmTP)GeFe(CO)$_4$	B	45	68.7	3.9	6.0	7.6	6.0	724	32.55	[(TmTP)Fe]$^+$
			(68.69)	(3.99)	(6.16)	(7.98)	(6.14)	742	1.16	[(TmTP)Ge]$^+$
								798	100.00	[(TmTP)Ge–Fe]$^+$
								882	1.16	[(TmTP)Ge–Fe(CO)$_3$]$^+$
								911	2.32	[(TmTP)Ge–Fe(CO)$_4$ + H]$^+$

[a] Abbreviations used: OEP = octaethylporphinato(2–); TpTP = *meso*-tetra-*p*-tolylporphinato(2–); TmTP = *meso*-tetra-*m*-tolylporphinato(2–). [b] Legend: A = toluene; B = heptane. [c] Calculated values are given in parentheses.

Table II. ^{1}H NMR Data[a]

complex	R^1	R^2	protons of R^1	multiplicity[b]/intens	δ	protons of R^2	multiplicity/intens	δ
(OEP)SnFe(CO)$_4$[c]	H	C_2H_5		s/4	10.88	CH_3	t/24	1.95
						CH_2	m/16	4.26
(TpTP)SnFe(CO)$_4$[d]	C_6H_4Me-*p*	H	*p*-CH_3	s/12	2.40		s/8	9.25
			m-H	s/4	7.24			
			m′-H	s/4	7.32			
			o-H	M/8	8.10			
(TmTP)SnFe(CO)$_4$[d]	C_6H_4Me-*m*	H	*m*-CH_3	s/12	2.32		s/8	9.21
			o-H	M/8	7.36			
			p-H	M/4	7.90			
			m-H	M/4	8.27			
(OEP)GeFe(CO)$_4$[d]	H	C_2H_5		s/4	10.42	CH_3	t/24	1.80
						CH_2	m/16	3.94
(TpTP)GeFe(CO)$_4$[d]	C_6H_4Me-*p*	H	*p*-CH_3	s/12	2.38		s/8	9.18
			m-H	s/4	7.22			
			m′-H	s/4	7.30			
			o-H	s/4	8.06			
			o′-H	s/4	8.14			
(TmTP)GeFe(CO)$_4$[d]	C_6H_4Me-*m*	H	*m*-CH_3	s/12	2.31		s/8	9.16
			m-H	M/8	7.35			
			o-H	M/8	8.07			

[a] Spectra recorded at 21 °C with $SiMe_4$ as internal reference; chemical shifts downfield from $SiMe_4$ defined as positive. [b] Legend: s = singlet; t = triplet; m = multiplet; M = broad peak. [c] Solvent C_5D_5N. [d] Solvent C_6D_6.

Table III. Characteristic Solid IR Data and UV–Visible Spectroscopic Data in Toluene

complex	IR data ν(C≡O), cm^{-1}			λ_{max}, nm ($10^{-4}\epsilon$) *B*(1,0)	*B*(0,0)	$\epsilon_{B(0,0)}/\epsilon_{B(1,0)}$	*Q*(2,0)	*Q*(1,0)	*Q*(0,0)
(OEP)SnFe(CO)$_4$	2019	1938	1905	368 (7.25)	441 (9.44)	1.30	558 (1.46)	592 (0.51)	
(TpTP)SnFe(CO)$_4$	2023	1943	1917–1905	350 (6.51)	453 (20.30)	3.12	540 (0.47)	585 (0.92)	630 (1.10)
(TmTP)SnFe(CO)$_4$	2022	1933	1925–1909	354 (5.73)	451 (23.16)	4.04	540 (0.35)	583 (1.02)	628 (1.20)
(OEP)GeFe(CO)$_4$	2023	1940	1912–1904	366 (7.12)	442 (9.52)	1.33	557 (1.38)	591 (0.49)	
(TpTP)GeFe(CO)$_4$	2026	1945	1919–1905	350 (6.42)	452 (20.26)	3.15	540 (0.47)	582 (1.00)	625 (1.05)
(TmTP)GeFe(CO)$_4$	2027	1944	1933–1911	351 (4.71)	454 (19.31)	4.10	540 (0.42)	582 (0.99)	627 (0.93)

calomel electrode (SCE) was used as the reference electrode and was separated from the bulk of the solution by a fritted-glass bridge. Controlled-potential electrolysis was performed in a bulk cell where the SCE reference electrode and the Pt wire counter electrode were separated from the test solution by fritted-glass bridges containing solvent and supporting electrolyte. A BAS 100 electrochemical analyzer was used to control the potential. Tetrabutylammonium hexafluorophosphate (TBA(PF_6)) was used as supporting electrolyte and was recrystallized in methylene chloride/hexane mixtures.

Spectroelectrochemical experiments were performed with an IBM Model EC 225 voltammetric analyzer coupled with a Tracor Northern 1710 holographic optical spectrometer/multichannel analyzer to obtain time-resolved spectral data. The Pt thin-layer cell that was used has been described elsewhere.[19]

Results

Spectroscopic Properties. Elemental analyses and mass spectral data of the complexes are shown in Table I and are in good agreement with the molecular formula (P)MFe(CO)$_4$. Mass

(19) Lin, X. Q.; Kadish, K. M. *Anal. Chem.* **1985**, *57*, 1498.

Table IV. Peak and Half-Wave Potentials (V vs. SCE) for the Electrode Reactions of (P)MFe(CO)$_4$ at Au and Pt Working Electrodes in CH_2Cl_2 and PhCN Containing 0.1 M TBA(PF_6)[a]

	CH_2Cl_2			PhCN		
	oxidn[b]	redn[b]		oxidn	redn	
compd	E_p(III)[c]	$E_{1/2}$(I)	$E_{1/2}$(II)	E_p(III)[c]	$E_{1/2}$(I)	$E_{1/2}$(II)
(TpTP)GeFe(CO)$_4$	0.58 (0.68)	−1.02 (−1.05)	−1.41 (−1.45)	0.51	−0.97	−1.43
(TpTP)SnFe(CO)$_4$	0.69 (0.79)	−1.00 (−1.00)	−1.38 (−1.39)	0.65	−0.94	−1.39
(TmTP)GeFe(CO)$_4$	0.56	−1.02	−1.41	0.47	−0.96	−1.42
(TmTP)SnFe(CO)$_4$	0.67	−0.97	−1.36	0.66	−0.91	−1.36
(OEP)GeFe(CO)$_4$	0.42 (0.48)	−1.29 (−1.26)	−1.75 (−1.72)	0.43	−1.22	−1.71
(OEP)SnFe(CO)$_4$	0.50 (0.59)	−1.24 (−1.23)	−1.70 (−1.69)	0.50	−1.17	−1.64

[a] Peaks I–III are identified in Figures 2 and 7. [b] Values in parentheses were measured at Pt. [c] Scan rate 0.20 V/s.

spectra of the germanium complexes show very weak molecular peaks (of relative intensity 0.63–2.32) corresponding either to the neutral or to the protonated form of the complexes. For the tin complexes, the molecular peak is only observed for (TmTP)SnFe(CO)$_4$. Otherwise, only peaks of lower m/e values appear. Parent peaks of both series are more often obtained by elimination of carbon monoxide or Fe(CO)$_4$. The most peculiar observation is made for the (TpTP)MFe(CO)$_4$ complexes since the parent peaks correspond to the transmetallic [(TpTP)Fe]$^+$ species.

Benzene or pyridine was used as a solvent for studying the ^{1}H NMR of the metal–metal-bonded complexes. The octaethylporphyrin derivative spectra show a singlet for the meso protons, a triplet for the methyl protons, and a multiplet for the methylenic protons (Table II). The last splitting shows that these protons are not magnetically equivalent and pentacoordination with the metal center raised above the porphyrin core can explain the shape.[20] (OEP)Sn^{II} is not air-stable but has still been characterized by NMR.[17] The methylenic protons of (OEP)Sn^{II} have the same shape as those in (OEP)SnFe(CO)$_4$, but the meso protons are more deshielded for the bimetallic complexes. This can be explained by the influence of the two metals which diminish the electron density on the macrocycle.

The tetraaryl compounds exhibit a singlet for the pyrrole proton resonance and three, four, or five signals for the *p*-MeC$_6$H$_4$(TpTP) or *m*-MeC$_6$H$_4$(TmTP) groups. Thus, the out-of-plane displacement of the tin or germanium ion in these species is clearly demonstrated by a doubling of the *o*-H and *m*-H peaks of the tetraarylporphyrin derivatives. There is a C_{4v} symmetry, and the doubling of the *o*-H and *m*-H peaks can be attributed to a highly distorted porphinato core and to a hindered rotation of the aryl rings induced by the presence of the CO ligands.

Infrared frequencies for the described complexes are listed in Table III. In the carbonyl stretching region, the IR spectra of all the compounds exhibit three bands. Two bands are sharp (at ~2019–2027 and 1933–1945 cm^{-1}) while the band at lowest energy (at ca. 1904–1933 cm^{-1}) is very broad and intense. The band patterns are quite similar to those of known tetracarbonyliron complexes.[21] On the basis of "local C_{3v}" symmetry for the Fe(CO)$_4$ fragments, three infrared-active carbonyl stretchings are predicted by group theory. The splitting of the lowest energy band in most complexes can indicate some lowering of the symmetry from C_{3v}.

Maximum wavelengths and molar absorptivities of each (P)GeFe(CO)$_4$ and (P)SnFe(CO)$_4$ complex are presented in Table III. The octaethylporphyrin complexes belong to the hyper class.[22,23] The complexes show two bands in the Soret region (350–453 nm) and two other bands that are red shifted with respect to the Soret band (540–630 nm). These absorption spectra are characteristic of p-type hyperporphyrins which contain main-group metals in a lower oxidation state. Sn(II), Pb(II), and Sb(III) porphyrins show similar spectra.[22,23]

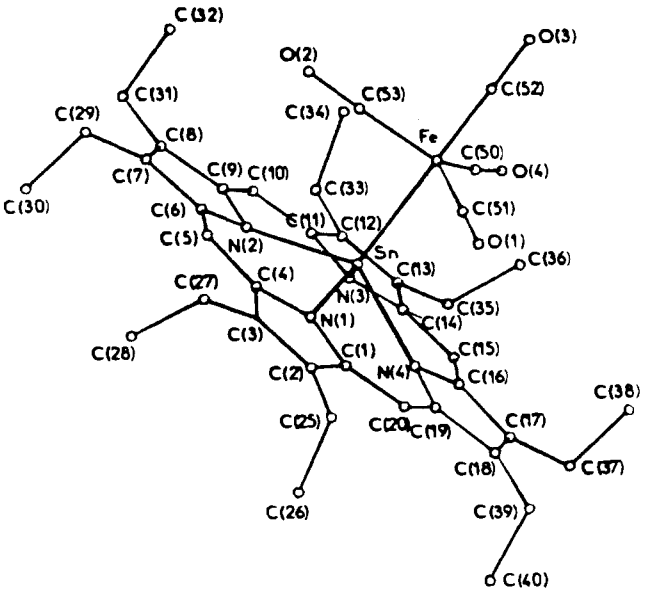

Figure 1. Single-crystal X-ray structure of (OEP)SnFe(CO)$_4$.

The ratio of molar absorptivities for two peaks of a given metalloporphyrin, $\epsilon_{B(0,0)}/\epsilon_{B(1,0)}$, usually depends on the porphyrin substituents and on the metal. For all of the complexes investigated in this study, the ratio is greater than unity and the UV–visible data suggest that the tin and germanium ions are in a low oxidation state.

Octaethylporphyrin complexes present a clear hyperporphyrin character since the ratio of $\epsilon_{B(0,0)}/\epsilon_{B(1,0)}$ is close to 1.0. On the other hand, absorption spectra of tetraaryl derivatives are not strikingly different from normal porphyrin spectra. They show two bands in the Soret region (350–460 nm) with an $\epsilon_{B(0,0)}/\epsilon_{B(1,0)}$ ratio that varies from 1.30 to 4.10. There are also three other bands that are red shifted with respect to the Soret band (540–630 nm).

Finally, the crystal structure of (OEP)SnFe(CO)$_4$ has been established by X-ray diffraction techniques[12] and is shown in Figure 1. The Sn coordination is square pyramidal with the iron in an axial position (Sn–Fe = 2.492 (1) Å) whereas the iron atom possesses C_{3v} symmetry (⟨Fe–C⟩ = 1.754 (5) Å). The Sn atom lies 0.818 (9) Å out of plane of the four nitrogen atoms, and the radius of the "central hole" is 2.028 (3) Å.

Reduction of (P)GeFe(CO)$_4$ and (P)SnFe(CO)$_4$. The electroreductions of each (P)MFe(CO)$_4$ complex were investigated in CH_2Cl_2 and PhCN containing 0.1 M TBA(PF_6). Each dimer undergoes two one-electron reductions. These reductions are reversible to quasi-reversible, and values of half-wave potentials are summarized in Table IV at Pt and Au electrodes. No significant differences in $E_{1/2}$ for reduction were observed between the two electrodes, indicating the absence of surface effects.

Figure 2 shows cyclic voltammograms for reduction of the four (TpTP)MFe(CO)$_4$ and (OEP)MFe(CO)$_4$ complexes in CH_2Cl_2 with 0.1 M TBA(PF_6). The potential difference between the first reduction (peak I) and second reduction (peak II) is 0.39 V for

(20) Busby, C. A.; Dolphin, D. *J. Magn. Reson.* **1976**, *23*, 211.
(21) Nakamoto, K. In *Infrared and Raman Spectra of Inorganic and Coordination Compounds*, 3rd ed.; Wiley: New York, 1978; Part III, and references therein.
(22) Buchler, J. W. In *The Porphyrins*; Dolphin, D., Ed.; Academic: New York, 1978; Vol. I, Chapter 10, and references therein.
(23) Gouterman, M. In *The Porphyrins*; Dolphin, D., Ed.; Academic: New York, 1978; Vol. III, Chapter 1, and references therein.

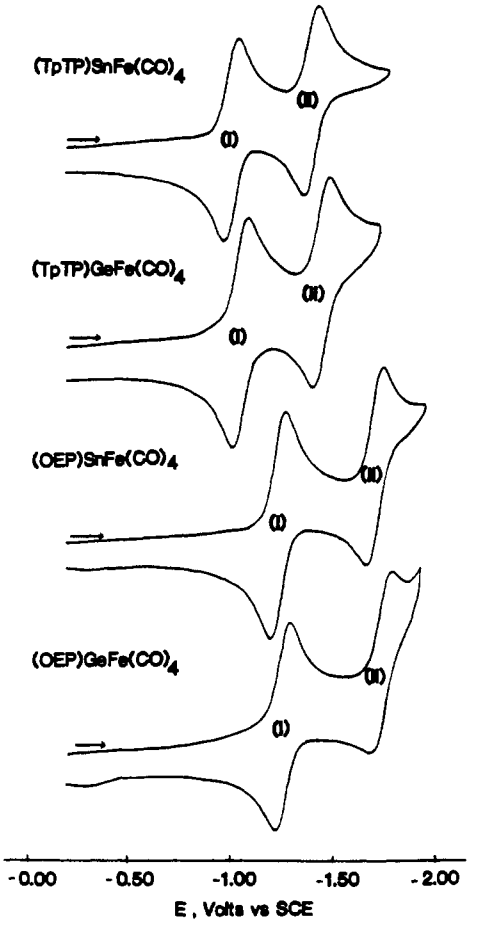

Figure 2. Cyclic voltammograms for reduction of the (TpTP)$MFe(CO)_4$ and (OEP)$MFe(CO)_4$ complexes at a Pt electrode in CH_2Cl_2 with 0.1 M $TBA(PF_6)$.

(TpTP)$SnFe(CO)_4$ and 0.40 V for (TpTP)$GeFe(CO)_4$ while for (OEP)$SnFe(CO)_4$ and (OEP)$GeFe(CO)_4$ these separations have increased to 0.46 V. Similar potential separations between peaks I and II are seen for (TmTP)$GeFe(CO)_4$ and (TmTP)$SnFe(CO)_4$ (Table IV) and are in agreement with an average separation of 0.44 ± 0.05 V for metalloporphyrins in which the two reductions have occurred at the porphyrin π ring system to give anion radicals and dianions.[24-26]

Fuhrhop, Kadish, and Davis[24] have also shown that the potentials for porphyrin π anion radical formation are linearly related to the electronegativity of the central metal ion and that the most positive reduction potentials are found for complexes having metal ions with the highest electronegativity. The absolute difference in reduction potentials between (P)$SnFe(CO)_4$ and (P)$GeFe(CO)_4$ ranges between 20 and 70 mV with the former complex being the most easy to reduce (see Table IV). This is consistent with the slightly higher electronegativity of Ge(II) (2.01) with respect to Sn(II) (1.96) and also suggests that the site of electroreduction occurs at the porphyrin π ring system.

The above conclusion regarding the site of electron addition was confirmed by thin-layer spectroelectrochemistry and controlled-potential electrolysis coupled with ESR. Potential-resolved thin-layer spectra were recorded after each one-electron reduction and are represented in Figures 3a and 4a for the two reductions of (TpTP)$SnFe(CO)_4$ in PhCN with 0.1 M $TBA(PF_6)$.

The most likely decomposition products of neutral (TpTP)-$SnFe(CO)_4$ are $[(TpTP)Sn]^{2+}$ and $[Fe(CO)_4]^{2-}$. Also, reduced (TpTP)$SnFe(CO)_4$ should result in the anion radical and/or

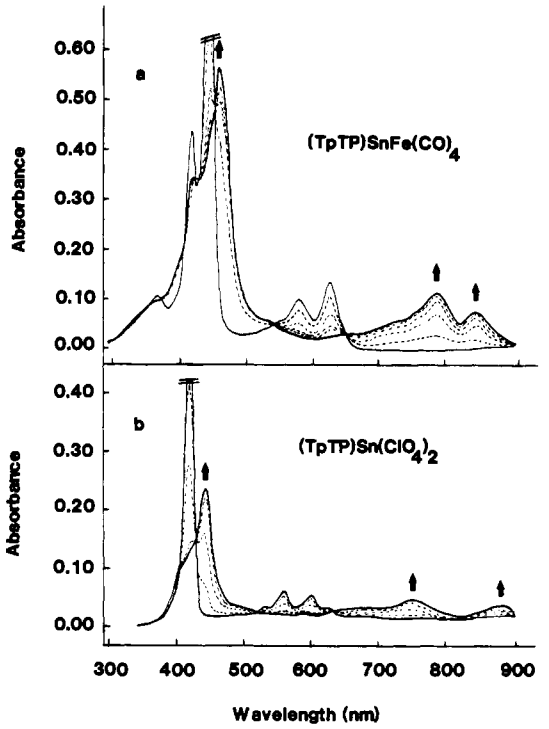

Figure 3. Potential-resolved thin-layer spectra recorded during the first reduction (in benzonitrile with 0.1 M $TBA(PF_6)$): (a) (TpTP)$SnFe(CO)_4$ at $E_{1/2}$ = −0.94 V; (b) (TpTP)$Sn(ClO_4)_2$ at $E_{1/2}$ = −0.82 V.

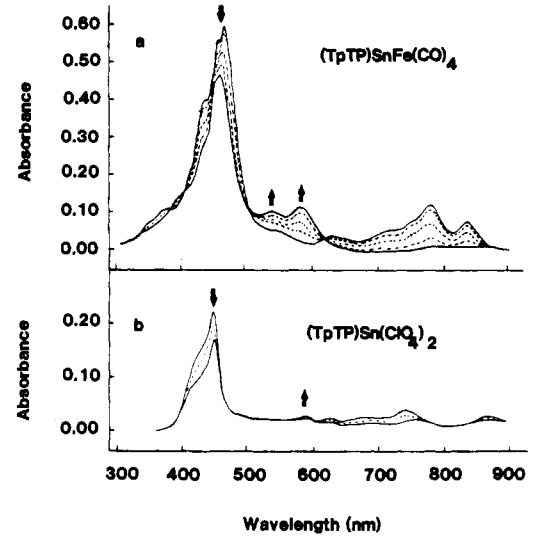

Figure 4. Potential-resolved thin-layer spectra recorded during the second reduction (in benzonitrile with 0.1 M $TBA(PF_6)$): (a) (TpTP)$SnFe(CO)_4$ at $E_{1/2}$ = −1.39 V; (b) (TpTP)$Sn(ClO_4)_2$ at $E_{1/2}$ = −1.36 V.

dianion of $[(TpTP)Sn]^{2+}$ after cleavage of the dimer. Thus, the spectra of singly and doubly reduced (TpTP)$Sn(ClO_4)_2$ were also obtained in order to investigate the stability of $[(TpTP)SnFe(CO)_4]^-$ and $[(TpTP)SnFe(CO)_4]^{2-}$ and at the same time to rule out spectral contributions from monomeric decomposition products. A cyclic voltammogram of (TpTP)$Sn(ClO_4)_2$ and $Na_2Fe(CO)_4$ is shown in Figure 5, and spectra of the singly and doubly reduced Sn(IV) complex are shown in Figures 3b and 4b.

The voltammograms of both (TpTP)$Sn(ClO_4)_2$ and $Na_2Fe(CO)_4$ in 0.1 $TBA(PF_6)$ are complicated. The former species is reduced in several steps, and the formation of chlorin or phlorin has been reported to be a product of the doubly reduced species.[27] In addition, a peak is observed on the first scan that is not present at the second or higher scans (see Figure 5b). Studies of this

(24) Fuhrhop, J.-H.; Kadish, K. M.; Davis, D. G. *J. Am. Chem. Soc.* **1973**, *95*, 5140.
(25) Kadish, K. M. *Prog. Inorg. Chem.* **1986**, *34*, 435–605.
(26) Felton, R. H.; Linschitz, H. *J. Am. Chem. Soc.* **1966**, *88*, 1113.
(27) Baral, S.; Hambright, P.; Neta, P. *J. Phys. Chem.* **1984**, *88*, 1595.

Table V. Maximum Absorbance Wavelengths (λ_{max}) and Corresponding Molar Absorptivities ($10^{-3}\epsilon$) of Neutral and Singly and Doubly Reduced (P)MFe(CO)$_4$ Complexes in PhCN Containing 0.1 M TBA(PF_6)

compd	λ_{max}, nm ($10^{-3}\epsilon$)					
(TpTP)GeFe(CO)$_4$	364 (11)	456 (165)	585 (10)	629 (13)		
[(TpTP)GeFe(CO)$_4$]$^-$	366 (11)	472 (54)	710 (3)	776 (5)	829 (4)	
[(TpTP)GeFe(CO)$_4$]$^{2-}$		470 (45)	589 (19)			
(TpTP)SnFe(CO)$_4$	369 (34)	454 (302)	588 (17)	634 (21)		
[(TpTP)SnFe(CO)$_4$]$^-$	369 (34)	468 (77)	790 (17)	849 (12)		
[(TpTP)SnFe(CO)$_4$]$^{2-}$		461 (60)	539 (14)	586 (16)		
(TmTP)GeFe(CO)$_4$	357 (21)	456 (90)	587 (5)	629 (6)		
[(TmTP)GeFe(CO)$_4$]$^-$	357 (20)	470 (31)	708 (2)	779 (3)	831 (2)	
[(TmTP)GeFe(CO)$_4$]$^{2-}$		474 (26)	596 (6)	725 (3)		
(TmTP)SnFe(CO)$_4$	362 (18)	453 (174)	584 (10)	630 (12)		
[(TmTP)SnFe(CO)$_4$]$^-$	362 (18)	467 (56)	635 (3)	704 (6)	785 (13)	842 (10)
[(TmTP)SnFe(CO)$_4$]$^{2-}$		466 (51)	590 (11)	636 (4)		
(OEP)GeFe(CO)$_4$	378 (37)	448 (265)	564 (38)	597 (29)		
[(OEP)GeFe(CO)$_4$]$^-$	383 (36)	454 (133)	637 (31)	692 (31)	788 (26)	
[(OEP)GeFe(CO)$_4$]$^{2-}$		457 (95)				
(OEP)SnFe(CO)$_4$	375 (47)	444 (123)	560 (31)	596 (11)		
[(OEP)SnFe(CO)$_4$]$^-$	375 (39)	448 (64)	637 (15)	691 (15)	799 (12)	
[(OEP)SnFe(CO)$_4$]$^{2-}$		457 (46)				

compound are under further investigation. However, of interest to this present study is the fact that no peaks due to [(TpTP)-Sn^{IV}]$^{2+}$ are observed as reduction products of (TpTP)SnFe(CO)$_4$. Likewise, no bands associated with reduced [(TpTP)Sn^{IV}]$^{2+}$ (Figures 3b and 4b) are observed upon controlled-potential reduction of (TpTP)SnFe(CO)$_4$ (Figures 3a and 4a). It should be noted, however, that the addition of $Na_2Fe(CO)_4$ to solutions of PhCN will lead to $NaHFe(CO)_4$ but no peaks for this species were observed during reduction of (TpTP)SnFe(CO)$_4$ nor were peaks for this species observed in the cyclic voltammograms for reduction of any other (P)MFe(CO)$_4$ complexes.

Figure 3a illustrates the potential-resolved spectra during the first reduction of (TpTP)SnFe(CO)$_4$. As the reduction proceeds, the Soret band, initially at 454 nm, shifts to 468 nm while significantly decreasing in intensity. The two peaks originally at 588 and 634 nm also decrease while new peaks appear at 790 and 849 nm. During reduction of (TpTP)Sn(ClO_4)$_2$ (Figure 3b) the Soret band, initially at 427 nm, shifts to 451 nm and decreases in intensity. The two bands at 557 and 598 nm disappear while bands typical of an anion radical are seen at 745 and 872 nm.

The second one-electron reduction of [(TpTP)SnFe(CO)$_4$]$^-$ occurs at $E_{1/2}$ = −1.39 V and yields the stable [(TpTP)SnFe-(CO)$_4$]$^{2-}$ species, whose spectrum is shown in Figure 4a. The Soret band of [(TpTP)SnFe(CO)$_4$]$^{2-}$ is located at 461 nm, and two broad absorption bands are seen at 539 and 586 nm. No absorption bands are observed at wavelengths higher than 600 nm. After back-electrolysis, the initial (TpTP)SnFe(CO)$_4$ spectrum is totally recovered. No decomposition of the dimer is observed after the addition of one or two electrons since this would generate either [(TpTP)Sn^{IV}]$^+$ or [(TpTP)Sn^{IV}]^0 and neither of these species are spectrally observed. The spectra of these last two species are given in Figure 3b and 4b and were generated from (TpTP)Sn(ClO_4)$_2$ by controlled-potential reduction.

The spectra of reduced (TpTP)SnFe(CO)$_4$ in Figures 3a and 4a are characteristic of porphyrin anion radicals and dianions.[26,28] Similar anion radical and dianion type spectra are also observed upon electroreduction of the other (P)MFe(CO)$_4$ complexes. These spectra are illustrated in Table V, which lists the wavelength maxima and molar absorptivities of the neutral complex and of the singly and doubly reduced species.

Figure 6 shows the low-temperature ESR signal for [(TpTP)GeFe(CO)$_4$]$^-$ and [(TpTP)SnFe(CO)$_4$]$^-$. These spectra were generated by controlled-potential reduction of the neutral complexes at −1.35 V in CH_2Cl_2 with 0.1 M TBA(PF_6). The two signals are typical of porphyrin anion radicals.[28] The reductions were reversible on the controlled-potential electrolysis time scale,

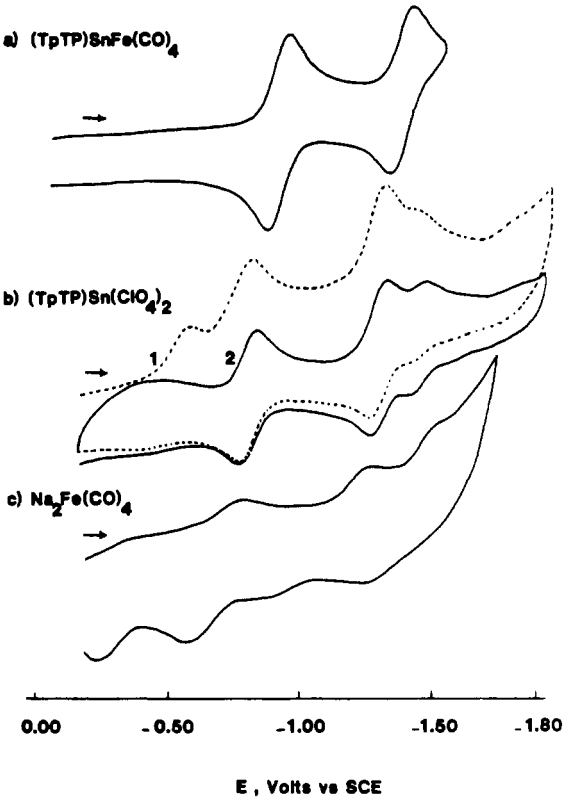

Figure 5. Cyclic voltammograms of (a) (TpTP)SnFe(CO)$_4$, (b) (TpTP)Sn(ClO_4)$_2$ on the first (---) and second (—) scan, and (c) $Na_2Fe(CO)_4$ at a Au electrode in PhCN with 0.1 M TBA(PF_6).

and upon application of a positive potential, the original diamagnetic species could be regenerated.

Similar behavior was observed for the other four investigated complexes. Thus, it appears that the addition of the first electron to (P)SnFe(CO)$_4$ and (P)GeFe(CO)$_4$ is invariably at the π ring system of the metalloporphyrin. This is in contrast to the case for both (L)Fe(CO)$_4$ and (P)InM(CO)$_3$Cp, where reduction occurs at the Fe(0) atom[29] and at the axial ligand,[8] respectively. The former reductions occur in a range of potentials between −1.6 and −2.1 V and depend upon the donor character of the bound L group.[29] While one might expect (P)M^{II}Fe(CO)$_4$ to exhibit these same electrode reactions, the addition of two electrons to

(28) Fajer, J.; Davis, M. S. In *The Porphyrins*; Dolphin, D., Ed.; Academic: New York, 1979; Vol. IV, Chapter 4.

(29) Connelly, N. G.; Geiger, W. E. *Adv. Organomet. Chem.* **1984**, *23*, 24.

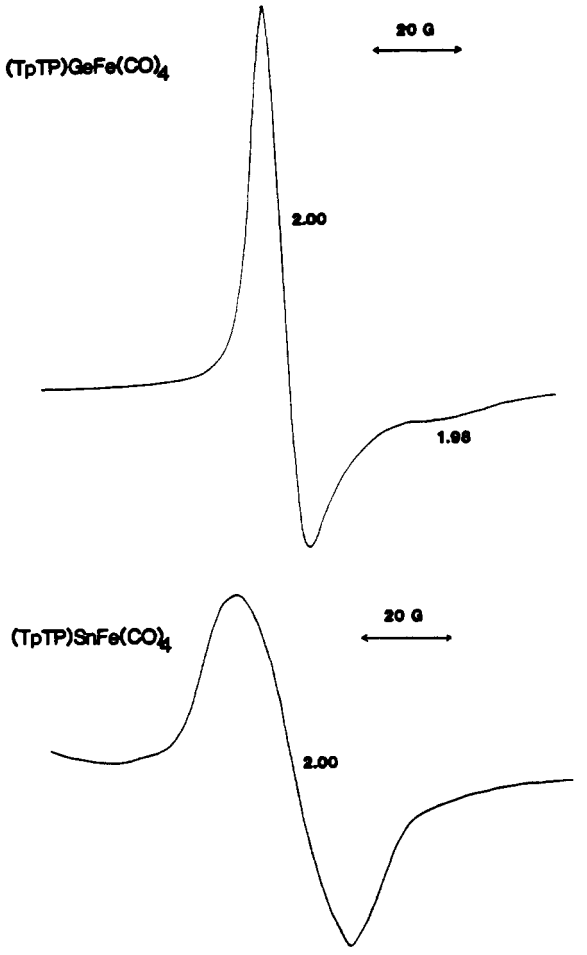

Figure 6. ESR signal recorded after the first reduction of (TpTP)-$GeFe(CO)_4$ and (TpTP)$SnFe(CO)_4$ in CH_2Cl_2 with 0.1 M $TBA(PF_6)$.

the porphyrin ring of $(P)M^{II}Fe(CO)_4$ will change the donor character of the metalloporphyrin such that extremely negative potentials would be needed for reduction of the iron carbonyl unit.

The differences in stability of reduced $(P)InM(CO)_3Cp$ (M = W, Mo) and $(P)MFe(CO)_4$ (M = Sn, Ge) seem to be clearly related to differences in the site of reduction between the two complexes. The σ-bonded complexes are extremely unstable after electroreduction, which occurs at a site localized at the metal–metal bond. In contrast, the $(P)MFe(CO)_4$ complexes are extremely stable, and in those cases the site of electroreduction is at the porphyrin π ring system. Since the Sn atom is removed by 0.81 Å from the plane of the porphyrin ring,[12] there is less interaction between the electron localized in the porphyrin π ring system and the metal–metal bond. This could account for the large increase in stability of these reduced complexes.

Oxidation of $(P)GeFe(CO)_4$ and $(P)SnFe(CO)_4$. Each bimetallic complex undergoes a single oxidation, which is chemically and electrochemically irreversible. This process involves the overall abstraction of two electrons and results in a cleavage of the metal–metal bond. Values of E_p for this reaction are dependent upon scan rate and are listed in Table IV at a scan rate of 0.20 V/s.

Figure 7 shows the oxidation of four $(P)SnFe(CO)_4$ and (P)-$GeFe(CO)_4$ complexes by cyclic voltammetry at a Au electrode in CH_2Cl_2 with 0.1 M $TBA(PF_6)$. All of the oxidations were irreversible in the sense that there were no coupled peaks associated with reduction of $[(P)MFe(CO)_4]^+$ or $[(P)MFe(CO)_4]^{2+}$. An apparent rereduction is observed in Figure 7 for (TpTP)$SnFe$-$(CO)_4$ and $(OEP)GeFe(CO)_4$, but these peaks actually correspond to the reduction of iron–carbonyl fragments formed upon cleavage of the dimeric unit.

Similar voltammograms were obtained for all six complexes, and peak potentials for the single oxidation (labeled peak III) at

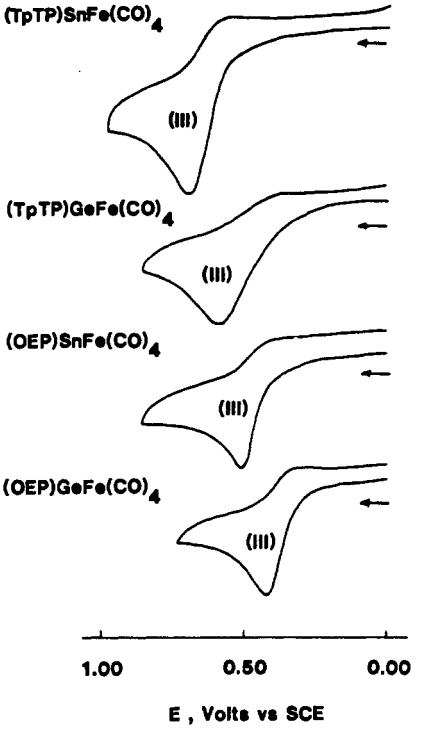

Figure 7. Cyclic voltammograms illustrating oxidation of the (TpTP)-$MFe(CO)_4$ and $(OEP)MFe(CO)_4$ complexes at a Au electrode in CH_2Cl_2 with 0.1 M $TBA(PF_6)$.

Au and Pt electrodes are listed in Table IV. As expected, the OEP complexes are easier to oxidize than the TpTP and TmTP complexes. Also, with a given porphyrin ligand the oxidation is easier for the Ge(II) than for the Sn(II) complex due to the higher electronegativity of the germanium atom.

The peak potential for oxidation of each $(P)MFe(CO)_4$ complex shifts in a positive direction with increase in scan rate. The slope of $\Delta E_p/\Delta \log v$ varies between 51 and 65 mV and is 53 mV for the oxidation of (TpTP)$SnFe(CO)_4$ in benzonitrile with 0.1 M $TBA(PF_6)$. This indicates an irreversible electron-transfer reaction in all cases. Irreversible waves are theoretically shifted by 0.0295 $V/\alpha n$ where αn is the electrochemical transfer coefficient.[30] Thus, the 53-mV shift of E_p for the oxidation of (TpTP)$SnFe(CO)_4$ corresponds to an $\alpha n = 0.56$. Irreversible oxidations were obtained for each complex, and the values of αn ranged between 0.58 and 0.67 for oxidation of $(P)GeFe(CO)_4$ at a Au electrode in CH_2Cl_2 and between 0.46 and 0.59 for the same series of oxidations at a Pt electrode in PhCN. These values were also calculated from the difference in $E_p - E_{p/2}$ by cyclic voltammetry and gave results that were equal within experimental error of that calculated from the shift of E_p with scan rate.

Rotating-disk voltammetry shows that the oxidation of each $(P)MFe(CO)_4$ complex is a diffusion-controlled process. The peak currents are proportional to the square root of the rotation rate, and plots of E vs. $\log [(i_d - i)/i]$ are linear. The slope of the plot for $(OEP)SnFe(CO)_4$ is 129.6 mV, which gives $\alpha n = 0.59$. This value is in good agreement with the αn value obtained by cyclic voltammetry on platinum. Figure 8 illustrates a rotating-disk voltammogram and cyclic voltammogram of (TpTP)$SnFe(CO)_4$ in PhCN with 0.1 M $TBA(PF_6)$. At a rotation rate of 1600 rpm the current maximum ratio of i_d(III) over i_d(I) was equal to 1.22. This value was generally larger than 1.0 for all of the compounds but approached 1.0 as the rotation rate increased. This is illustrated in Figure 9a for reduction of $(OEP)SnFe(CO)_4$.

The ratio of i_p(III) over i_p(I) by cyclic voltammetry was also equal to or greater than 1.0 (see Figure 8b), depending on the compound and the scan rate. However, in all cases the ratio increased to values larger than 1.0 as the scan rate was decreased.

(30) Nicholson, R. S.; Shain, I. *Anal. Chem.* **1964**, *36*, 706.

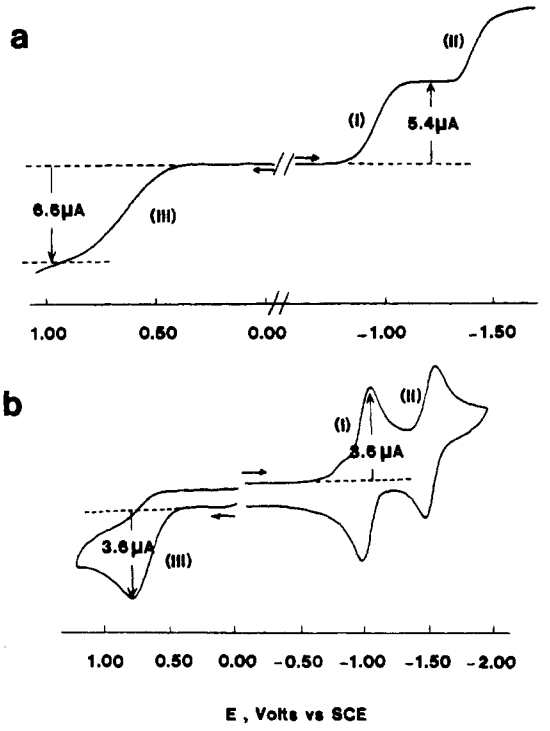

Figure 8. (a) Rotating-disk voltammogram (ω = 1600 rpm) and (b) cyclic voltammogram (v = 0.20 V/s) of (TpTP)SnFe(CO)$_4$ at a Pt electrode in PhCN with 0.1 M TBA(PF_6).

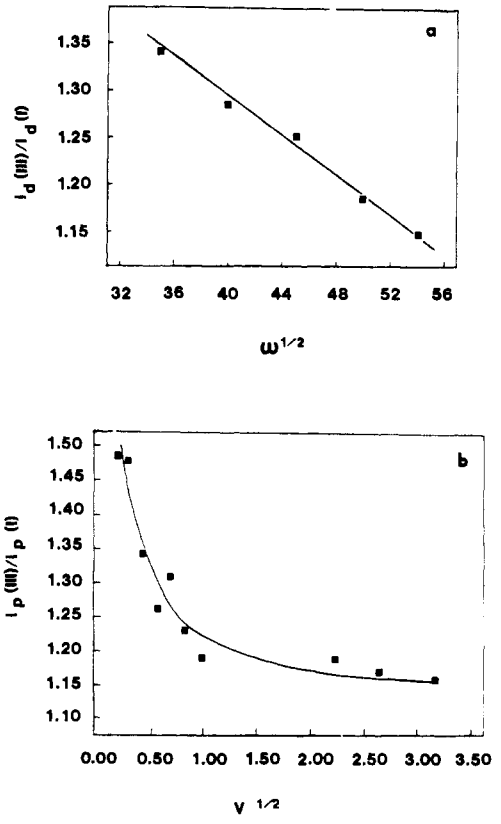

Figure 9. Ratio of maximum currents for (a) the oxidation and reduction of (OEP)SnFe(CO)$_4$ by rotating-disk voltammetry and (b) the oxidation and reduction of (OEP)GeFe(CO)$_4$ by cyclic voltammetry. Processes I and III are identified in Figure 8.

This is shown in Figure 9b for the oxidation and reduction of (OEP)GeFe(CO)$_4$ at a Au electrode in PhCN. These data suggest an ECE type mechanism where the second electron transfer is cut off at high rotation rates (rotating-disk voltammetry) or high potential scan rates (cyclic voltammetry).

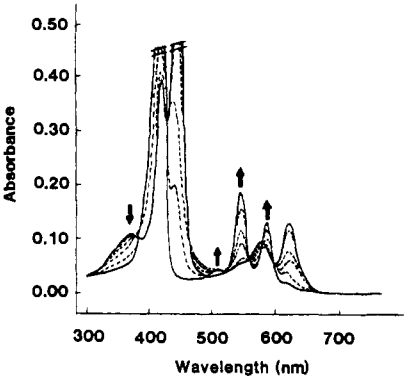

Figure 10. Potential-resolved thin-layer spectra for the conversion of (TpTP)SnFe(CO)$_4$ to (TpTP)Sn(PF_6)$_2$ during electrooxidation in PhCN with 0.1 M TBA(PF_6).

The primary oxidation products of (P)MFe(CO)$_4$ are $[(P)M^{IV}]^{2+}$ and $Fe_3(CO)_{12}$. These fragments are formed after the global abstraction of 2.3 electrons from (P)MFe(CO)$_4$ and cleavage of the bimetallic complex as postulated in Scheme I. The first step in the electrooxidation is the irreversible abstraction of one electron from (P)MFe(CO)$_4$ (reaction 1). This rate-controlling step is followed by a cleavage of the metal–metal bond as shown in reaction 2. Cleavage of the metal–metal bond is not especially rapid as evidenced by the fact that the maximum currents by rotating-disk voltammetry are less than those predicted for an ECE type mechanism where each of the electrochemical steps involve one electron. On the other hand, the irreversibility of the initial rate-determining electron-transfer step prevents a determination of the chemical rate constant in reaction 2. This electrochemical irreversibility also leads to oxidations without a coupled reverse peak as is predicted by theory.[30]

Scheme I

$$(P)M^{II}Fe(CO)_4 \xrightarrow{-e^-} [(P)M^{III}Fe(CO)_4]^{\bullet+} \quad (1)$$

$$[(P)M^{III}Fe(CO)_4]^+ \rightarrow [(P)M^{III}]^+ + Fe(CO)_4^{\bullet+} \quad (2)$$

$$[(P)M^{III}]^+ \xrightarrow{-e^-} [(P)M^{IV}]^{2+} \quad (3)$$

$$Fe(CO)_4^{\bullet} \rightarrow {}^1/_3[Fe_3(CO)_{12}]^{\bullet-} \xrightarrow{-e^-} {}^1/_3Fe_3(CO)_{12} \quad (4)$$

Evidence for Scheme I for (TpTP)SnFe(CO)$_4$ and the other (P)MFe(CO)$_4$ complexes comes from coulometric values of n, which are slightly larger than 2.0 (a theoretical value of 2.3 is predicted) and from identification of $[(P)M^{IV}]^{2+}$ and $Fe_3(CO)_{12}$ as major products of the oxidation. Both $[(P)M^{IV}]^{2+}$ and $Fe_3(CO)_{12}$ fragments were monitored by cyclic voltammetry, UV–visible spectra, and IR spectra after electrooxidation.

The only porphyrin spectroscopically identified as a product of (TpTP)SnFe(CO)$_4$ oxidation is $[(TpTP)Sn^{IV}]^{2+}$. Other iron carbonyl fragments most likely are present as transient decomposition products (see IR data in the following section), but the nature of these products was not identified in this study. Also, there were no well-defined isosbestic points in spectra taken during the electrooxidation (see Figure 10). This is consistent with the mechanism presented in Scheme I and indicates the presence of intermediates in the reaction.

Figure 11a shows voltammograms for the oxidation and rereduction of (TpTP)SnFe(CO)$_4$ in PhCN with 0.1 M TBA(PF_6). The initial oxidation occurs at E_p = 0.58 V and is coupled to two reduction peaks at −0.82 and −0.40 V. Both of these reductions are not present on initial negative-potential scans. The reduction at −0.82 V can be attributed to $[(TpTP)Sn^{IV}]^{2+}$, which is generated after cleavage of the dimer. A peak for reduction of (TpTP)Sn(ClO_4)$_2$ in 0.1 M TBA(PF_6) occurs at approximately the same potential (see Figure 11b). The small current at −0.82 V in Figure 11a is not unusual and is due to the fact that the generated

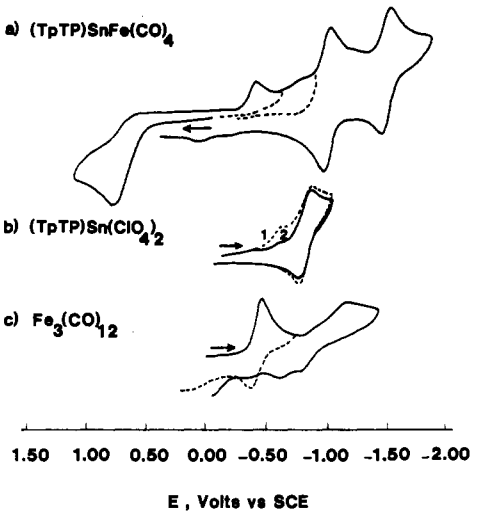

Figure 11. Cyclic voltammograms for the oxidation of (a) (TpTP)-$SnFe(CO)_4$, (b) (TpTP)$Sn(ClO_4)_2$ on first (---) and second (—) scan, and (c) Fe_3CO_{12} at a Au electrode in PhCN with 0.1 M $TBA(PF_6)$ (scan rate 0.20 V/s).

$[(TpTP)Sn^{IV}]^{2+}$ can diffuse away from the electrode before rereduction.

The reduction peak at −0.40 V is only present after oxidation of $(TpTP)SnFe(CO)_4$ and shifts cathodically with increase in scan rate. This suggests a chemical reaction following electron transfer. This wave can be attributed to reduction of $Fe_3(CO)_{12}$, which, as shown in Scheme I, is a product of the cleavage reaction. The fact that larger currents are obtained for $Fe_3(CO)_{12}$ reduction than for $[(TpTP)Sn]^{2+}$ reduction is due to the fact that $Fe_3(CO)_{12}$ should have a larger diffusion coefficient than $[(TpTP)Sn]^{2+}$ and that the former compound (which is reduced at more positive potentials) has less time to diffuse away before reduction.

A voltammogram of $Fe_3(CO)_{12}$ is shown in Figure 11c. On the first scan $Fe_3(CO)_{12}$ is reduced in a quasi-reversible reaction at $E_{1/2} = -0.42$ V. However, the shape of the voltammogram changes after several scans. Reduced $Fe_3(CO)_{12}$ decomposes to give $Fe(CO)_5$ and other carbonyls, and this results in changes in the shape of the voltammogram.[31]

Other anionic iron carbonyl fragments can react with $[(P)Ge^{IV}]^{2+}$ or $[(P)Sn^{IV}]^{2+}$ to generate some form of Sn(II) or Ge(II) dimer, and this is suggested by thin-layer spectra taken after controlled-potential rereduction at −0.45 V. There was no clear evidence by cyclic voltammetry for the re-formation of $(TpTP)SnFe(CO)_4$ when $Fe_3(CO)_{12}$ was added to fresh solutions of (TpTP)$Sn(ClO_4)_2$, but this reaction was suggested by UV–visible spectra, which resemble those of the starting species. Also, the voltammetric wave of $Fe_3(CO)_{12}$ remained reversible in the presence of (TpTP)$Sn(ClO_4)_2$ and was irreversible only by thin-layer voltammetry. This leads to the conclusion that $Fe_3(CO)_{12}$ is not the only carbonyl product formed upon cleavage of the dimer. Evidence for this conclusion also comes from IR spectroscopy.

Figure 12 shows IR spectra recorded during bulk electrolysis of $(TpTP)SnFe(CO)_4$ in CH_2Cl_2 with 0.1 M $TBA(PF_6)$. The initial spectrum (Figure 12a) has absorbances close to those given in Table III, but the values are slightly shifted due to the different solvent systems. A peak at 1715 cm^{-1} appears as the reaction proceeds (Figure 12b). This peak then begins to decrease and disappear (Figure 12c). The identity of this intermediate is not known. It is not $Fe_3(CO)_{12}$ or $(H)Fe(CO)_4$ but may be a product formed after reaction of the carbonyl and the solvent.

In summary, this paper presents the first physical and electrochemical characterization of binuclear donor–acceptor com-

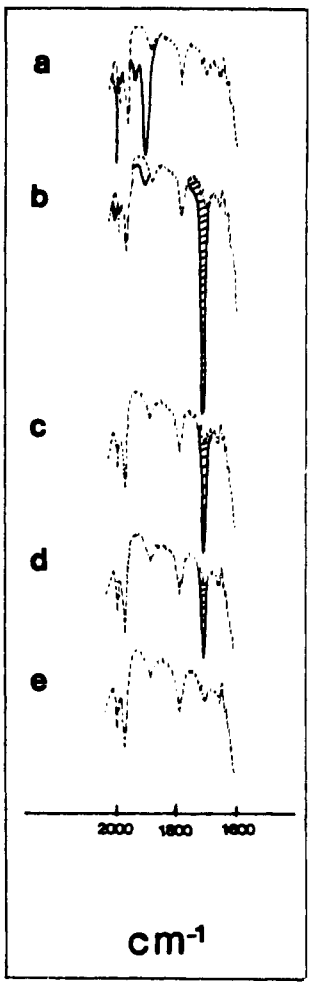

Figure 12. IR spectra recorded (a) before, (b)–(d) during, and (e) after complete electrooxidation of $(TpTP)SnFe(CO)_4$ in CH_2Cl_2 with 0.1 M $TBA(PF_6)$. The shaded peak occurs at an absorption of 1715 cm^{-1}.

plexes involving metalloporphyrins. It also presents the first electrochemical studies of Sn(II) and Ge(II) porphyrins. Binuclear complexes with both of these low-oxidation-state central metals are irreversibly oxidized with a concomitant cleavage of the metal–metal bond. On the other hand, all of the binuclear complexes can be reversibly reduced by two single-electron additions. The reduced products are remarkably stable even after the addition of two electrons to the complex. This is in contrast to binuclear σ-bonded porphyrins of the type (P)In–ML, where ML is a metal carbonyl fragment.[8] However, the singly reduced σ-bonded bimetallic complexes are only stable on a short time scale and the doubly reduced σ-bonded dimers very rapidly decompose into porphyrin and metalate ion fragments.[8] This is due perhaps to the fact that reduction of the σ-bonded species occurs at an orbital directly involved in the metal–metal bond. This is not the case for $(P)SnFe(CO)_4$ and $(P)GeFe(CO)_4$, which are reduced at the porphyrin π ring system.

It is not known if the observed stabilities of the reduced complexes are due to the presence of the Ge(II) or Sn(II) metal ions or if they are related in part to the characteristics of the $Fe(CO)_4$ fragment, which is bound to the metalloporphyrin. However, studies of other σ-bonded and donor–acceptor complexes are now in progress and should help to answer these questions. Especially interesting will be results for the trimetallic $[(P)In]_2Fe(CO)_4$, whose synthesis has been reported in the literature.[7]

Acknowledgment. The support of the National Science Foundation (K.M.K., Grant CHE-8215507) is gratefully acknowledged. K.M.K. and R.G. also acknowledge support of a joint grant from NSF/CNRS (Grant INT-8413696).

(31) El Murr, N.; Chaloyard, A. *Inorg. Chem.* **1982**, *21*, 2206.